MNRAS **000**, 000–000 (0000) Preprint 11 April 2016 Compiled using MNRAS LATEX style file v3.0

Hot accretion flow with radiative cooling: state transitions in black hole X-ray binaries

Mao-Chun Wu[1]⋆; Fu-Guo Xie[2]; Ye-Fei Yuan[1]; Zhaoming Gan[2]
[1]*Key Laboratory for Research in Galaxies and Cosmology, Department of Astronomy, University of Science and Technology of China, Hefei, Anhui, 230026, China;*
[2]*Key Laboratory for Research in Galaxies and Cosmology, Shanghai Astronomical Observatory, Chinese Academy of Sciences, 80 Nandan Road, Shanghai 200030, China*

arXiv:1604.02283v1 [astro-ph.HE] 8 Apr 2016

11 April 2016

ABSTRACT
We investigate state transitions in black hole X-ray binaries through different parameters by using two-dimensional axisymmetric hydrodynamical simulation method. For radiative cooling in hot accretion flow, we take into account the bremsstrahlung, synchrotron and synchrotron-self Comptonization self-consistently in the dynamics. Our main result is that the state transitions occur when the accretion rate reaches a critical value $\dot{M} \sim 3\alpha\ \dot{M}_{\rm Edd}$, above which cold and dense clumpy/filamentary structures are formed, embedded within the hot gas. We argued this mode likely corresponds to the proposed two-phase accretion model, which may be responsible for the intermediate state of black hole X-ray binaries. When the accretion rate becomes sufficiently high, the clumpy/filamentary structures gradually merge and settle down onto the mid-plane. Eventually the accretion geometry transforms to a disc-corona configuration. In summary our results are consistent with the truncated accretion scenario for the state transition.

Key words: accretion, accretion discs – black hole physics – hydrodynamics: HD – ISM: jets and outflow

1 INTRODUCTION

The accretion of matter onto black holes, where a huge amount of energy (both radiative and kinematic) is liberated out, is the key process in black hole X-ray binaries (BHBs) and active galactic nuclei (AGNs). Interestingly, it is argued that both BHBs and AGNs can be divided into two different broad states/types. This is most evident in BHBs, where two states with distinctive spectral and timing properties are identified (see e.g. Zdziarski & Gierlinski 2004; Remillard & McClintock 2006; Belloni 2010 for recent reviews on the state classifications and their observational properties). As the source entering its outburst, generally it will first go through a hard state, which is fainter but with a hard power-law spectrum. The thermal component is highly suppressed in this state. As it brightens, it will enter into a soft state, in which the spectrum is characterized by a thermal component, supplemented with a weak power-law tail. Between these two standard states, there also exist a hybrid one, where the thermal and power-law components are comparable. We call it intermediate state. In AGNs, although less clear, more pieces of evidences are gathered recently to propose that the bright AGNs are analogy to BHBs in their soft states, while the low-luminosity AGNs (LLAGNs) are analogy to BHBs in their hard states (e.g. Ho 2008; Antonucci 2012; Done 2014).

As widely accepted, the basic theoretical picture of these two states is the truncated accretion – jet model (Esin et al. 1997; Yuan et al. 2005; see Yuan & Narayan 2014 for the latest review). In this model, the geometrically thin, optically thick, cold disc (Shakura & Sunyaev 1973; hereafter SSD) is believed to be truncated at a certain radius $R_{\rm tr}$, inside which it is replaced by a hot accretion flow such as the advection-dominated accretion flows (ADAFs; Narayan & Yi 1994, 1995; Abramowicz et al. 1995) or the luminous hot accretion flow (LHAF; Yuan 2001, 2003; Yuan et al. 2007; Xie & Yuan 2012). Additionally there is also a jet component, which is believed to be connected to the hot accretion flow (Fender et al. 2004; Wu et al. 2013). With this configuration, observationally the system will be in the hard state. As the accretion rate increases, $R_{\rm tr}$ becomes smaller. Eventually when $R_{\rm tr}$ is smaller than the innermost stable circular orbit (ISCO), i.e. the whole accretion is now a cold disc and the system will be in the soft state. The readers are referred to Yuan & Narayan (2014) for the most recent

⋆ Email: maochun@ustc.edu.cn (MCW), fgxie@shao.ac.cn (FGX)

© 0000 The Authors

review of the theory of hot accretion flows, including its dynamics, radiation, and the applications to observations.

Although non-radiative numerical simulations on hot accretion flows have been investigated for years (hydrodynamic [HD]: e.g. Stone, Pringle & Begelman 1999; Igumenshchev & Abramowicz 1999, 2000; Yuan, Wu & Bu 2012; magnetohydrodynamic [MHD]: e.g. Stone & Pringle 2001; Hawley, Balbus & Stone 2001; Igumenshchev, Narayan & Abramowicz 2003; De Villiers et al. 2003; Machida et al. 2004; Narayan et al. 2012; Yuan, Bu & Wu 2012), only until very recently the dynamical importance of radiative cooling on the hot accretion flow has been examined through numerical simulations (e.g. Machida et al. 2006; Fragile & Meier 2009; Ohsuga et al. 2009; Yuan & Bu 2010; Ohsuga & Mineshige 2011; Dibi et al. 2012; Li, Ostriker & Sunyaev 2013; Sądowski & Narayan 2015). Moreover, the theoretical interpretation of the state transition still lacks direct support from numerical simulations. The first step, to our knowledge, is taken by Das & Sharma (2013), where they studied the effects of radiative cooling on hot accretion flow. They found that, there exist a certain critical density (depend on the viscous parameter α), above which the whole simulation domain will be in a globally stable two-zone configuration, i.e. an outer cold disc and an inner hot accretion flow. Such geometric configuration has been expected for almost two decades (e.g. Esin et al. 1997).

Apart from its success, several shortages of their work could be noted. Firstly, only bremsstrahlung emission is considered, while in reality the innermost regions ($R < 20-30\,R_{\rm s}$, where $R_{\rm s} = GM_{\rm BH}/c^2$ is the Schwarzschild radius of the black hole; cf. Fig. 2 and Section 3.2.2) of hot accretion flow are cooled by synchrotron and its Comptioization (Narayan & Yi 1995; hereafter NY95). Secondly, they adopt a optically-thin assumption and the radiative transfer is not taken into account, which should not be the case when state transition occurs. Thirdly, an one-temperature (ion temperature $T_{\rm i}$ equals electron temperature $T_{\rm e}$ at every location) structure is assumed, which is known to be incorrect (e.g. NY95; Moscibrodzka et al. 2009) for most cases in hot accretion flows.

In this paper, we investigate the dynamical impacts of radiative cooling in hot accretion flows by using two dimensional radiative HD simulations, aiming at understanding the state transitions in BHBs (and the evolution of AGN activity). The main improvement of our work is that, besides the bremsstrahlung, both the synchrotron radiation and its Comptioization are considered, following the treatment of NY95[1]. Moreover, the impacts of gas pressure to magnetic pressure ratio β, the ratio of electron temperature to ion temperature $T_{\rm e}/T_{\rm i}$, on the evolutionary stages of accretion flows, are also investigated.

Another motivation of this work is to verify, from state transition simulations, the existence of LHAF (Yuan 2001, 2003; Yuan et al. 2007; Yuan & Bu 2010; Xie & Yuan 2012), a hot accretion flow with accretion rate and radiative efficiency higher than those of typical ADAFs. This new solution is promising for the understanding of bright hard state (Yuan et al. 2007; Ma 2012). Besides, with even higher accretion rate, analytical investigations of the height-integrated one-dimensional solutions indicate that thermal instability could be triggered. Consequently the accretion flow will be possibly in two-phase (a type II LHAF branch, see Yuan 2003; Xie & Yuan 2012, 2016), i.e. numerous cold clumps will be formed, embedded in the hot gas. This two-phase accretion flow may relate to the intermediate state in BHBs (Yang et al. 2015). Eventually as the accretion rate increases further, the cold clumps may grow, merge and settle down to the mid-plane, resulting the usual SSD. Together with the low-density hot medium above the cold disc, the disc-corona configuration is recovered, and the accretion system enters into a soft state.

The structure of this paper is as follows. In Section 2, we describe our numerical method and the treatment on various radiative cooling mechanisms in hot accretion flow. The main results are described in Section 3. Finally Section 4 is devoted to a brief summary and discussions.

2 METHOD

2.1 Basic hydrodynamic equations

In our numerical simulations, we use the ZEUS-2D code (Stone et al. 1992) to solve the basic hydrodynamic equations in spherical coordinates (R, θ, ϕ):

$$\frac{{\rm d}\rho}{{\rm d}t} + \rho\nabla\cdot\mathbf{v} = 0, \tag{1}$$

$$\rho\frac{{\rm d}\mathbf{v}}{{\rm d}t} = -\nabla P_{\rm tot} - \rho\nabla\phi + \nabla\cdot\mathbf{T}, \tag{2}$$

$$\rho\frac{{\rm d}({\rm e}/\rho)}{{\rm d}t} = -P_{\rm gas}\nabla\cdot\mathbf{v} + \mathbf{T}^2/\mu - Q^-_{\rm rad}. \tag{3}$$

Here ρ is the mass density, $\mathbf{v}$ is the gas velocity, $P_{\rm tot} \equiv P_{\rm gas} + P_{\rm mag}$ is the total (gas+magnetic) pressure, $\mathbf{T}$ is the anomalous stress tensor. A pseudo-Newtonian gravitational potential (Paczyński & Wiita 1980) is adopted, $\phi = -GM_{\rm BH}/(R - R_{\rm s})$. Besides, for an ideal gas, the internal energy e can be expressed as, $e = P_{\rm gas}/(\gamma - 1)$, where $\gamma = 5/3$.

The stress tensor $\mathbf{T}$ is now widely believed to be associated with MHD turbulence driven by the magneto-rotational instability (MRI, see Balbus & Hawley 1998 for a review). However, since our simulation is hydrodynamic, we follow the conventional strategy, to use the α-viscosity description (Shakura & Sunyaev 1973), Following Stone, Pringle & Begelman (1999), we include the non-zero azimuthal components of $\mathbf{T}$,

$$T_{r\phi} = \mu R\frac{\partial}{\partial R}\left(\frac{v_\phi}{R}\right), \tag{4}$$

$$T_{\theta\phi} = \frac{\mu\sin\theta}{R}\frac{\partial}{\partial\theta}\left(\frac{v_\phi}{\sin\theta}\right). \tag{5}$$

Here, the viscous coefficient $\mu = \nu\rho$ and the kinematic coefficient $\nu \propto r^{1/2}$, which is similar to the standard α-description (Shuakura & Sunyaev 1973).

Although global large-scale magnetic field may exist in the hot accretion flow, we here neglect it since our simulations are hydrodynamic (see Section 5 for discussions

[1] Note that, the NY95 approach is also adopted in the general relativistic radiative MHD simulations by Fragile & Meier (2009). However, they assumed $T_{\rm e} = T_{\rm i}$, i.e. an one-temperature accretion flow.

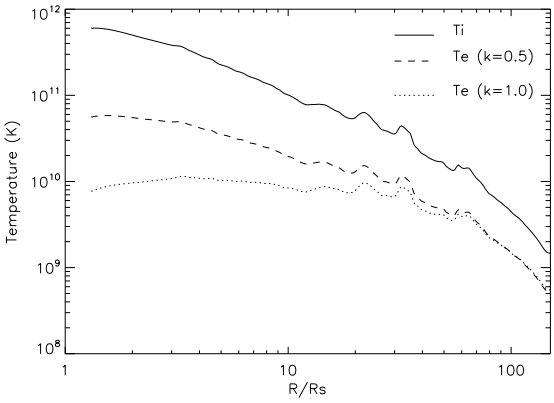

Figure 1. Ion temperature $T_{\rm i}$ and electron temperature $T_{\rm e}$ as a function of radius for cases with $k = 0.5$ and $k = 1$. The ion temperature is taken in fiducial **Run A** (see Table 1) at a quasi-steady state before considering radiative cooling.

on this point.). The local and randomly-oriented (tangled) magnetic field is determined through the plasma β parameter $\beta = P_{\rm gas}/P_{\rm mag}$. Consequently the total pressure can be expressed as $P_{\rm tot} = P_{\rm gas} + P_{\rm mag} = (1+\beta)/\beta\, P_{\rm gas}$. MHD numerical simulations of hot accretion flow indicate that, the value of β is not a constant, but varies with time and location (r, θ) within the simulation domain. Moreover, the average value of β likely depends on the magnitude of the net initial magnetic field (e.g. Stone & Pringle 2001; Hawley & Krolik 2001; Hawley et al. 2001; Beckwith et al. 2008. See Yuan & Narayan 2014 for review.). For simplicity we assume β is a constant.

The hot accretion flow is two-temperature (NY95), with electron temperature is much lower than ion in the innermost regions of the accretion flow, due to the fact that both the strong radiative cooling of electrons and different adiabatic index between electrons and ions (e.g. Narayan, Mahadaven & Quataert 1998; Yuan & Narayan 2014). We use the following formulae to mimic the results from height-integrated numerical calculations (NY95; Xie et al. 2010),

$$T_{\rm e} = \frac{T_{\rm i}}{(R/R_0)^{-k} + 2.0}, \tag{6}$$

where $k > 0$ is a tuning parameter and R_0 is the density maximum location of the initial torus (see Section 2.3 for the torus setup). In other words, we assume $T_{\rm e} \approx 0.3 T_{\rm i}$ at large radii ($r > 100\ R_{\rm s}$), and $T_{\rm e}$ can be highly suppressed (compared to $T_{\rm i}$) within $\sim 20\ R_{\rm s}$, where most of the radiation are emitted. Fig. 1 shows T_i and T_e as a function of radius for $k = 1$ and $k = 0.5$, the ion temperature plotted here is when the accretion flow gets to a quasi-steady state without adding radiative cooling. For a direct comparison, the radiative cooling of the bremsstrahlung emission at larger radii will be about a factor of $\sqrt{T_{\rm i}/T_{\rm e}} \approx \sqrt{3}$ lower, compared to those one-temperature simulations. On the other hand, for the dense clumps/filaments in our simulations, we underestimate the electron temperature because the clumps will be nearly one-temperature because of the strong energy exchange/coupling between electrons and ions.

2.2 Radiative cooling rate $Q^-_{\rm rad}$

We now provide the numerical formulae to derive the radiative cooling rate $Q^-_{\rm rad}$. Technically there are several treatments on the radiation, e.g. some researchers employ the flux-limited diffusion approximation to solve the radiation energy equation (Ohsuga et al. 2009). Here we take a different and also simplified approach to calculate all the radiative cooling terms. We note that the radiative processes in hot accretion flow include the bremsstrahlung, synchrotron, and the Comptonization (the seed photons are mainly the synchrotron photons, whose energy is much lower compared to that of bremsstrahlung photons.). The radiative cooling rate can then be expressed as,

$$Q^-_{\rm rad} = Q^-_{\rm brem} + Q^-_{\rm syn} + Q^-_{\rm syn,C}. \tag{7}$$

Here, $Q^-_{\rm brem}$ is the bremsstrahlung emission including both the electron-ion and electron-electron collisions (Eq. 3.4 in NY95).

Optically thin synchrotron radiation is emitted mainly at the local self-absorption peak frequency ν_c, below which the synchrotron emission is self-absorbed. Once the ν_c is determined at each location, we adopt a simplified formula (Eq. 3.18 in NY95) to estimate the synchrotron emission,

$$Q^-_{\rm syn} \approx \frac{2\pi}{3c^2} k T_{\rm e}(R) \frac{\nu_c^3(R)}{R}. \tag{8}$$

The above formula ensures that the integral of $Q^-_{\rm syn}$ over the entire accretion flow roughly equals to the total cooling radiation that reaches infinity (NY95). For the estimation of ν_c, we also follow the approach of NY95, with a slight modification. At radius R, the emission volume is revised to $2 \times H \times \Delta S$, where H is the scale height and ΔS is the surface area, instead of $4/3\ \pi R^3$. We then equate the synchrotron emission to the Rayleigh-Jeans blackbody emission from the surface of that volume. The net effect of this modification is to replace the R of eq. 3.14 in NY95 with $3H$, i.e. the surface density plays its role in determining ν_c.

One key process is the Compton scattering within the hot accretion flow. In this work we use the Compton enhancement factor η (Dermer, Liang & Canfield 1991) which is determined by the electron energy, the seed photons, the geometry of the Compton region and also the effective optical depth $\tau_{\rm eff}$. In the calculation of $\tau_{\rm eff}$, we adopt coefficients that correspond to a disc configuration and seed photon energy at 1 eV (Dermer et al. 1991; Eq. 3.19 in NY95). Moreover, since we do not do any integrations in the calculation of either synchrotron or Comptonization, we take ν_c as the mean seed photon energy. The radiative cooling rate due to the Comptonized synchrotron emission is,

$$Q^-_{\rm syn,C} = (\eta(T_{\rm e}, \nu_c, \tau_{\rm eff}) - 1)\ Q^-_{\rm syn}. \tag{9}$$

Two notes should be emphasized. First, all these formulae are based on the local Comptonization approximation which is crude and additional corrections should be made (e.g. Yuan, Xie & Ostriker 2009; Xie et al. 2010; Niedźwiecki et al. 2012). Second, the radiative transfer of the optically thin medium has been approximately taken into account under this approach, although we can not quantitatively estimate how goodness it is. We devote it to future work.

Since we investigate accretion flow with moderately high accretion rate, so cold clumps with large optical depth is expected. In order to take this effect into account, we define

Table 1. Model Parameters and Simulation Properties

Run	$\rho_{\max}/\rho_0$	β	k	$t_{\rm stop}$ [(a)]	$\dot{M}/\dot{M}_{\rm Edd}$ [(b)]
A	1.0	10	1.0	9.0	0.06
A1	0.5	10	1.0	8.0	0.03
A2	0.1	10	1.0	5.0	0.006
B	1.0	100	1.0	5.0	0.06
B1	1.0	1	1.0	5.0	0.06
E	0.5	10	0.5	5.0	0.03
E1	0.5	10	...[(c)]	5.0	0.03

(a) The whole physical simulation time $t_{\rm stop}$ in unit of the orbital period at $R_0 = 100\ R_{\rm s}$.
(b) The net accretion rate at location $2\ R_{\rm s}$ at time 1.4 orbits, when the whole accretion flow is in a quasi-steady state.
(c) In this case, we set $T_{\rm e} = T_{\rm i}$.

$\tau_{\rm es}$ the electron scattering optical depth in θ direction, from disc midplane $\theta = \pi/2$ to the local location θ. And also $\tau_{\rm abs}$ is the absorption optical depth. If the value of $\tau_{\rm abs}$ exceeds $\sim 1/3$ (arbitrarily set), we will correct the high-optical-depth issue, the following formulae is adopted (Hubeny 1990; see also NY95),

$$Q^-_{\rm rad} = \frac{4\sigma T_{\rm e}^4}{H}\ \frac{1}{\left(3\tau/2 + \sqrt{3} + 1/\tau_{\rm abs}\right)}. \qquad (10)$$

Here $\tau = \tau_{\rm abs} + \tau_{\rm es}$ is the total optical depth. $\tau_{\rm abs}$ can be approximated as (cf. Eq. 3.33 in NY95),

$$\tau_{\rm abs} = \frac{H}{4\sigma T_{\rm e}^4}\ \left(Q^-_{\rm brem} + Q^-_{\rm syn} + Q^-_{\rm syn,C}\right). \qquad (11)$$

2.3 Initial conditions

The initial setup is an equilibrium torus around a stellar mass black hole, with mass $M_{\rm BH} = 10\ M_\odot$. The torus structure is described as (Papaloizou & Pringle 1984),

$$\frac{P_{\rm gas}}{\rho} = \frac{(\gamma-1)GM_{\rm BH}}{\gamma R_0}\left[\frac{R_0}{R} - \frac{1}{2}\left(\frac{R_0}{R\sin\theta}\right)^2 - \frac{1}{2d}\right]. \qquad (12)$$

Here $R_0 = 100R_{\rm s}$ is the radius of the torus center (density maximum $\rho_{\max}$), d is the distortion of the torus. Additionally the torus is embedded in a low density medium. The density of these ambient gas density is $\rho_{\rm amb} = 1\times10^{-4}\ \rho_{\max}$. The specific angular momentum of the tours equals to the Keplerian angular momentum at R_0. We include the randomly-oriented magnetic fields in the simulations through plasma parameter β.

Different parameters are used to depict the accretion flow. The viscosity parameter α is fixed to 0.01, which is a typical value of current numerical simulations (e.g. Hawley et al. 2011; Mckinney et al. 2012); The ratio of gas pressure to magnetic pressure β; The maximum density $\rho_{\max}$ in the torus center which determines the quantity $\dot{M}$ in units of Eddington accretion rate ($\dot{M}_{\rm Edd} \equiv 10\ L_{\rm Edd}/c^2$, where $L_{\rm Edd}$ is the Eddington luminosity); Parameter k denotes the ratio of electron temperature to ion temperature. The parameters are summarized in table 1, columns (2) to (6) give the maximum density in the center of torus (in units of ρ_0, $\rho_0 \equiv 0.77\times10^{-6}{\rm g\cdot cm^{-3}}$), plasma parameter β, k, the total run time of the simulation (in units of orbital time at radius of $R_0 = 100R_{\rm s}$), and mass accretion rate $\dot{M}$ (in units of $\dot{M}_{\rm Edd}$).

2.4 Numerical methods

The public ZEUS-2D code (Stone & Norman 1992) are used in this work to solve the basic hydrodynamic equations. The shear stress and the radiative cooling are considered. The radiative cooling term is treated explicitly. The Courant–Friedrichs–Lewy condition for the radiative cooling is not taken into account. Instead, a sub-cycle technique is adopted for regions with high density (in the cold clumps), i.e. whenever the radiative cooling time-step is smaller than the time-step used for the hydrodynamic equations, we sub-cycle that. The radiative terms are repeatedly at the smaller time-step until one hydrodynamical time-step has elapsed for the purpose of saving computational time.

In our simulations, the inner and outer boundary (in radial direction) of the computational domain are set as, $R_{\rm in} = 1.3\ R_{\rm s}$ and $R_{\rm out} = 400\ R_{\rm s}$. We use outflow boundary conditions at these two boundaries so that mass is allowed to flow out of the computational domain but not into it. In the angular direction, the axis symmetric boundary condition is taken.

We followed the treatment of Stone et al. (1999) for the grid setup, i.e. logarithm in both the radial and the angular directions. More specifically, we choose in radial direction $(\triangle r)_{i+1}/(\triangle r)_i = \sqrt[N_r-1]{10}$ with N_r grid points per decade in radius. To resolve the cold clumps (and also the possible think disk) near the equator, we adopt non-uniform angular zones with $(\triangle\theta)_j/(\triangle\theta)_{j+1} = \sqrt[N_\theta-1]{4}$ for $0 \le \theta \le \pi/2$, and $(\triangle\theta)_{j+1}/(\triangle\theta)_j = \sqrt[N_\theta-1]{4}$ for $\pi/2 \le \theta \le \pi$. This gives a refinement by a factor of 4 in the angular grid zones between the poles and equator. The standard resolution is $N_{\rm r} = 128$ and $N_\theta = 80$, giving a grid with a total size of 334×160 zones. **The standard resolution gives the minimum grid of $\Delta r = 0.015R_{\rm s}$ and $\Delta\theta = 0.5^\circ$.** We have also computed a high resolution model with $N_r \times N_\theta = 128\times160$ (total 334×320). We caution that although the resolution is high enough to resolve the cold clumps formed near the equatorial plane, it is still insufficient to resolve clumps possibly formed at high altitude. Simulation with higher resolution is computationally expensive, which is beyond the scope of current work.

Technically, we first run the simulation (of the equilibrium torus) without radiative cooling. After the accretion flow enters a quasi-steady state, we then start to include the radiative cooling.

3 RESULTS

As summarized in Table 1, we have run seven HD simulations with different model parameters. We take **Run A** ($\alpha = 0.01$, $\beta = 10$, $k = 1.0$) as the fiducial run. The accretion time is in the units of the orbital period at radius $R_0 = 100\ R_{\rm s}$ in all models. We will first present results of this fiducial model to provide a general picture of our simulations, and then will go further to discuss the influences of individual model parameters. Note that the dynamical impact of the viscosity parameter α on hot accretion flows is well-known and easy to understand (see e.g. Stone, Pringle & Begelman 1999; Igumenshchev & Abramowicz 1999, 2000 for cases without radiation; Yuan & Bu 2010; Das & Sharma 2013 for cases with radiation), and we omit to discuss it here.

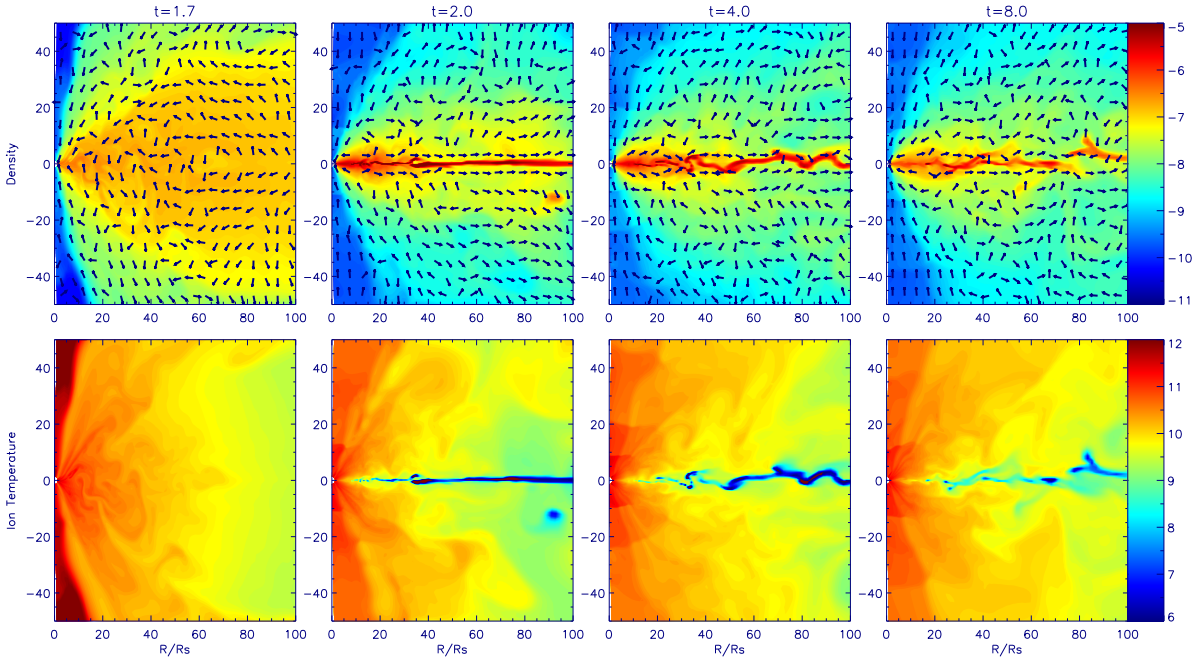

Figure 2. The logarithmic density (over-plotted with poloidal directions of the velocity as arrows) and temperature, for **Run A**. Panels from left to right show time at $t = 1.4, 2.0, 4.0, 8.0$, respectively.

3.1 Fiducial Run A

When the accretion flow reaches a quasi-steady state ($t = 1.4$ orbits), a representative of hard state in BHBs, we start to include the radiative cooling. Very quickly the state transition is triggered. If initially we setup with a very low density torus and the radiative cooling is weak (dynamically un-important), then such state transition will not happen at all. At a later time, $t = 2.0$, the whole accretion flow is now dominated by a cold, geometrically thin accretion disc and surrounded by a hot tenuous media, similar to the disc-corona configuration. This is likely a representative of the soft state. For completeness, we also present the results at $t = 4.0$ and $t = 8.0$, where the mass accretion rate is reduced gradually, because there is no continuous mass supply in our simulations.

To better understand the detailed structure of the accretion flow, Fig. 2 shows the density (upper panels) and ion temperature (bottom panels) for the four representative times as mentioned before and the density panels over-plotted with poloidal velocity field. At time $t = 1.4$, the accretion flow is globally geometrically thick with high temperature. Moreover, it is turbulent inflow near the equatorial plane, and outflow above certain altitude (see Yuan, Wu & Bu 2012 and references therein). At time $t = 2.0$, the cold, dense, geometrically thin accretion flow extends to radii $R > 100\ R_s$. After this stage, the dynamical structures of thin disc becomes turbulent as shown in the right two panels of Fig. 2. This is because there is no continuous mass supply in our simulations. Consequently as the system evolves, the gas density reduces, and the radiative cooling becomes less important. In other words, if we run the simulation for sufficiently long time, the accretion flow will eventually return back to a hot accretion flow, i.e. a transition from soft state to hard state. Note that, a soft-to-hard state transition is realized in **Run A1**, where the initial density and consequently the accretion rate are lower (cf. Fig. 6).

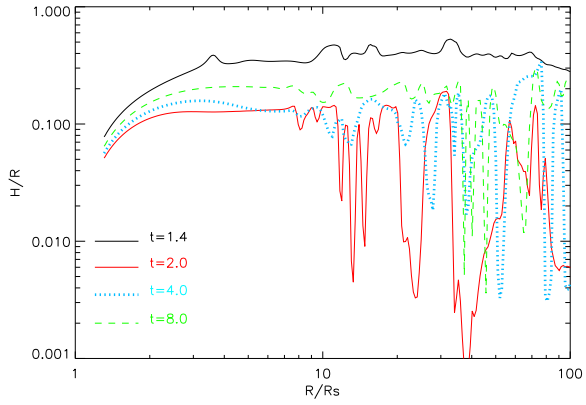

Figure 3. The aspect ratio H/R ($H \approx c_s/\Omega_K$) at the equatorial plane versus radius for **Run A**. The black solid, red solid, blue dotted and green dashed curves are respectively, correspond to the time $t = 1.4$, 2.0, 4.0, 8.0.

Fig. 3 shows the ratio of disc scale-height to radius H/R, as a function of radius. The disc scale-height is defined as, $H \approx c_s/\Omega_K$, where c_s is the sound speed and Ω_K is the Keplerian angular velocity. For simplicity, we only calculate the aspect ratio at the mid-plane. The black solid, red solid, blue dotted and green dashed curves show H/R at time $t =$ 1.4, 2.0, 4.0 and 8.0, respectively. For technical reasons we

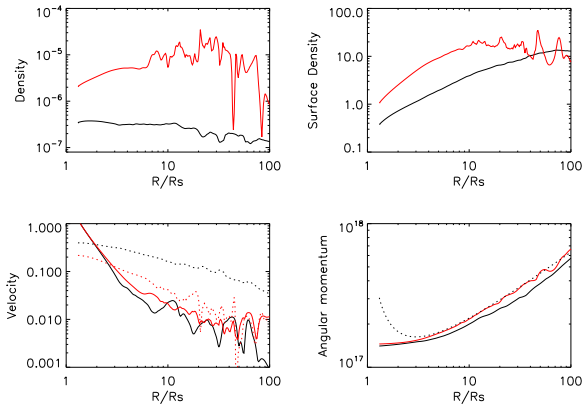

Figure 4. Radial scaling of time-averaged physical quantities for **Run A**. From left to right, upper to lower are the density, surface density, velocity and angular momentum, respectively.In each panel, colors denote different evolution time, the black color lines denotes $t = 1.4$ and red color line denotes $t = 2.0$. The density, surface density and angular momentum are in units of cgs. Only the velocities are in units of light speed. In the velocity panel, the solid lines denote radial velocity and dotted lines denote sound speed. In the angular momentum panel, dotted line represents the Keperlian angular momentum.

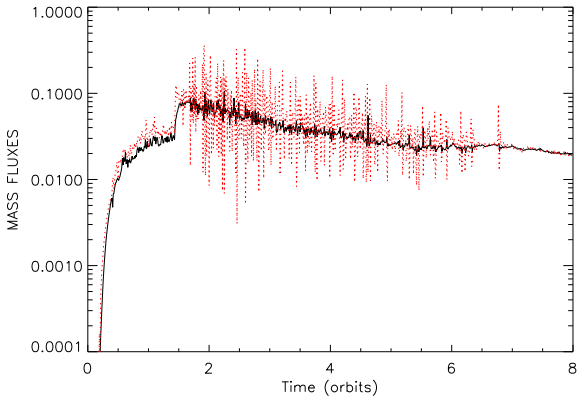

Figure 5. Mass accretion rate $\dot{M}$ (in units of Eddington accretion rate) at $R = 2\ R_s$ (black solid line) and $R = 10\ R_s$ (red dotted line), as a function of time (in units of the orbital time at R_0) for **Run A1**.

take the accretion flow with $H/R > 0.1$ as hot accretion flow and $H/R < 0.01$ as cold disc. From this definition, the accretion flow is a hot, geometrically thick disc at time $t = 1.4$, where the truncated radius $R_{tr} > 100\ R_s$, this stage is corresponded to the hard state. At time $t = 2.0$ when radiative cooling is taking into account, numerous cold components are formed (see also Fig. 2), almost represents a cold disc which is truncated at radius $\approx 10\ R_s$. Inside the truncated radius the accretion flow remains hot. As accretion rate decreases, the truncated radius become larger gradually, $R_{tr} \approx 25\ R_s$ at time $t = 4.0$ and $R_{tr} \approx 35\ R_s$ at time $t = 8.0$. This results is consistent with previous works (e.g. Das & Sharma 2013).

Fig. 4 shows the time averaged radial structures of the accretion flow at the equatorial plane, time is averaged over a duration of 0.1 orbits. In each panel, the black and red lines correspond to time $t = 1.4$ (the typical non-radiative hot accretion flow, likely the hard state) and $t = 2.0$ (the radiative accretion flow, likely the soft state), respectively. It is clear that each variable at hard state can be described by a simple radial power-law distribution, the density scales as $\rho \propto r^{-0.3}$, the surface density scales as $\Sigma \propto r^{-3/2}$, the radial velocity scales as $v_r \propto r^{-3/2}$ and the angular momentum scales as $l \propto r^{0.5}$.

After considering of the radiative cooling, the accretion flow change significantly in comparison with non-radiative model. The density increases by nearly two orders of magnitude, while the surface density increases by only a factor of ~ 10 due to the reduction in the disc thickness. Besides, it should be point out that the cold disc in our simulation is highly different from the standard SSD model, although its rotational velocity is Keplerian (bottom right panel in Fig. 4), the profiles in density, surface density, temperature as well as velocities deviate from predictions in SSD (Shakura & Sunyaev 1973; Frank, King & Raine 2003). Most notably, the radial velocity is very high in cold accretion flow. There are several reasons for these results. Firstly, the opacity we adopt for the cold disc is not the Kramers' law. Secondly, the treatment for the optically thick disc is still very crude. We expect it will eventually become the SSD, if several technical problems are solved, i.e. the radiative cooling will be well-treated, and more importantly, the resolution (especially in the angular direction) will be highly improved. Global simulations of SSD is beyond the scope of this work.

3.2 The dependence on $\dot{M}$

The first and most apparent parameter is the accretion rate, or density of the initial torus, which will control the whole mass supply of the system. To investigate its effect, we run another two simulations with different accretion rate including **Run A1** with $\dot{M} = 0.03\ \dot{M}_{Edd}$ and **Run A2** with $\dot{M} = 0.006\ \dot{M}_{Edd}$. We use a slightly high numerical resolution (total: 334×320) in **Run A1** to discern filament structures. Our simulation results indicate that the critical mass accretion rate is about $\sim 0.03\ \dot{M}_{Edd}$, below this critical accretion rate the hard-to-soft state transition can not happen. For example, the whole accretion flow remains purely hot (not shown here) throughout the evolution time for **Run A2** ($\dot{M} = 0.006\ \dot{M}_{Edd}$). **Run A2** is similar to the non-radiative hydrodynamical simulations (e.g. Stone, Pringle & Begelman 1999). In other words, the mass accretion rate is lower than the critical value, thus the radiative cooling of this model are sufficiently low which results in very weak dynamical impact.

Fig. 5 shows the evolution of the net mass accretion rate (see Stone, Pringle & Begelman 1999 for definition) at radius of $2R_s$ (black solid line) and $10R_s$ (red dotted line) in units of Eddington accretion rate for **Run A1**. The net accretion rate increases by a factor of ~ 2 after considering the radiation cooling. As the gas enters into the central black hole, the mass accretion rate decreases due to no supplementary matter. At time $t \gtrsim 6.5$ orbits, the net accretion rate $\sim 0.02\ \dot{M}_{Edd}$, which is below the critical rate, so the accretion flow enters into a hard state again. This may

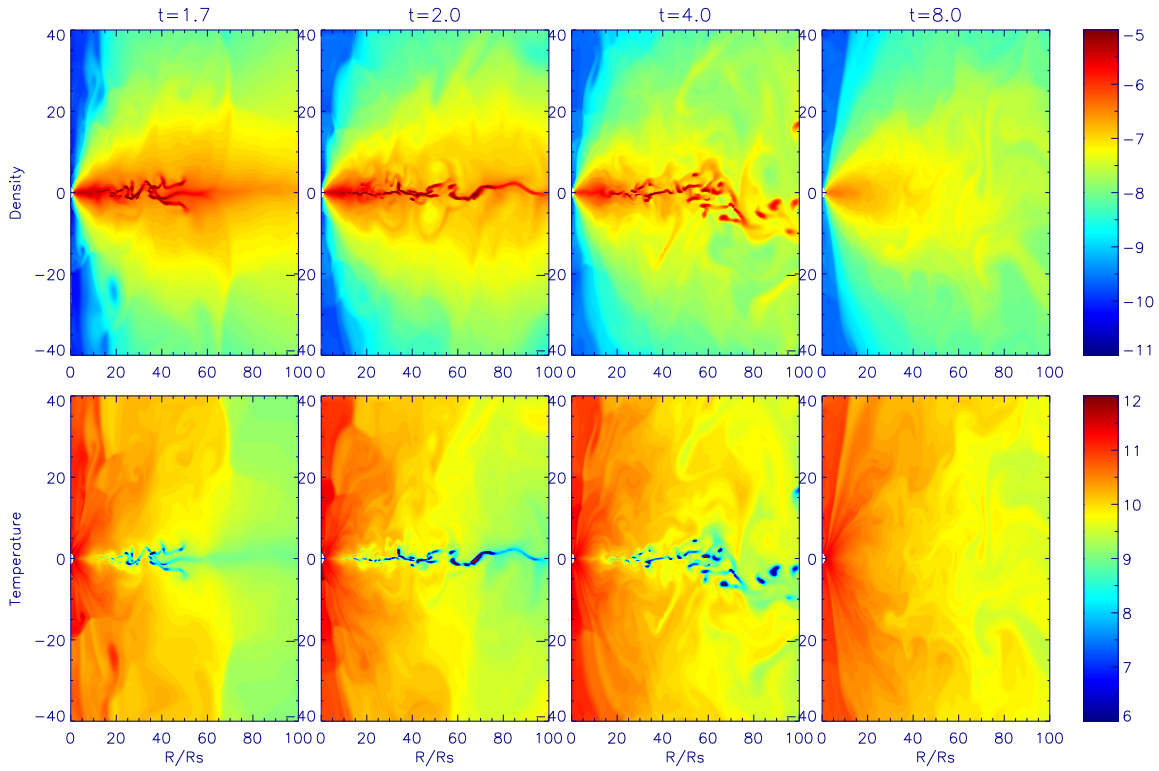

Figure 6. The density (upper panels) and ion temperature (lower panels) in logarithmic scale for **Run A1** (cf. Table 1). The panels show at different time, from left to right, t = 1.7, 2.0, 4.0, 8.0, respectively.

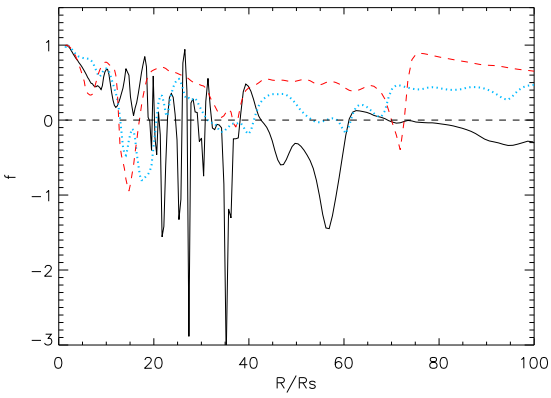

Figure 7. The snapshot (t = 1.7) of advection factor f for **Run A1** at different angular locations, $\theta = 90°$ (black solid line; equatorial plane), $\theta = 70°$ (blue dotted line) and $\theta = 50°$ (red dashed line) respectively.

be similar to a soft-to-hard state transition in the decay of BHBs outburst. Moreover, fluctuation in the mass accretion rate at radius of $R = 10\ R_s$ is weaker again at time $t \gtrsim 6.5$, mainly because of the disappeared cold clumps.

Fig. 6 shows the density and temperature of the accretion system of **Run A1**, from left to right panels corresponding to time 1.7, 2.0, 4.0 and 8.0 orbits, respectively. From this plot, obviously there is no conventional cold thin SSD, but instead of filamentary and sometimes clumpy cold and dense structures except for the rightmost panel. These cold and dense structures are concentrated to lower altitude, but clearly they are highly turbulent, without any sign of settling down onto the mid-plane. The truncated radius of this model $R_{tr} \approx 35\ R_s$ at time $t = 2.0$ (not show picture here) is the same as **Run A** which has same accretion rate $\dot{M} \sim 0.03\ \dot{M}_{Edd}$ at time t = 8.0. This result is highly close to the two-phase LHAF model proposed by Yuan (2003) (see also Xie & Yuan 2012 and Yang et al. 2015 for more discussions). It is clear that at time $t = 8.0$ the accretion flow becomes hot and dilute again, namely in hard state.

3.2.1 **Run A1***: luminous hot accretion flow?*

Fig. 7 shows advection factor of hot accretion flow at time t = 1.7 in **Run A1**. The advection factor is defined as (Narayan & Yi 1994; Yuan & Narayan 2014),

$$f \equiv \frac{Q_{adv}}{Q_{vis}} = 1 - \frac{Q^{-}_{rad}}{Q_{vis}}, \qquad (13)$$

where $Q_{adv} \equiv \rho d(e/\rho)/dt + p\nabla \cdot \mathbf{v} \equiv \rho T dS/dt$ (S is the entropy) is the so-called advection term. In this plot, the curves represent advection factor f at different angular locations, $\theta = 90°$ (black solid; equatorial plane), $\theta = 70°$ (blue dotted) and $\theta = 50°$ (red dashed), respectively. The advection factor is negative at radii larger than 40 R_s although the flow is still in hard state. This is exactly the case of type I luminous hot accretion flow (e.g. Yuan 2001, 2003), which the radiative

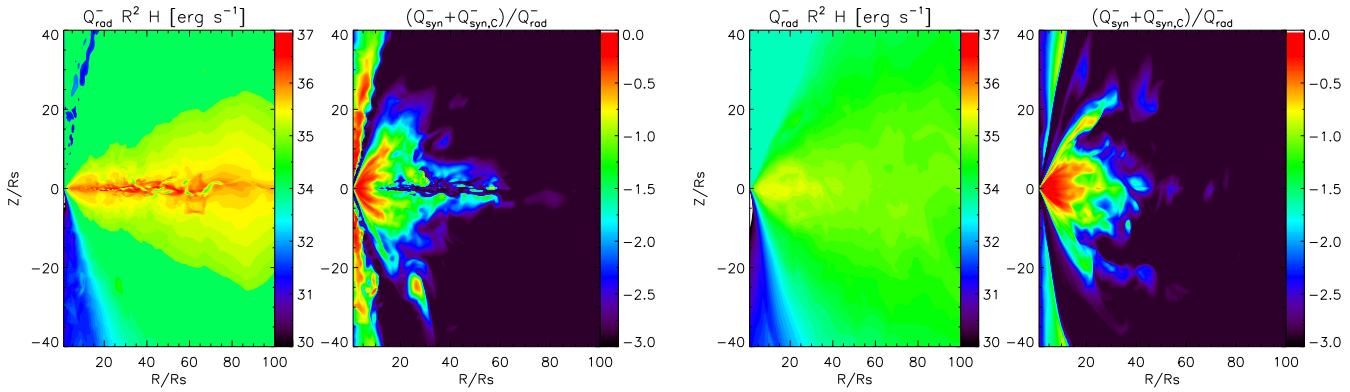

Figure 8. The logarithmic radiative cooling term for **Run A1** over the period 1.8−2.0 (left two panels) and 7.8−8.0 (right two panels). The first/third panel shows the total radiative cooling rate multiplied by R^2 H and the second/fourth panel shows ratio between Comptonized synchrotron radiative cooling rate and radiative total cooling rate.

cooling is very strong even larger than viscous heating, but the advection term plays a heating role, rather than a cooling role, so the accretion flow remains hot.

3.2.2 radiative cooling in accretion flows

One advantage of **Run A1** is that, it shows the purely hot accretion flow (at $t \gtrsim 6.5$), the LHAF (at $t \approx 1.7$), and the two-phase accretion flow (at $1.8 \lesssim t \lesssim 6.5$). We here investigate in detail the contributions of different radiative cooling processes. We show in Fig. 8 the total radiation cooling rate (multiplied by the volume R^2H, i.e. $Q^-_{\rm rad}R^2H$) and the ratio of the Comptonized synchrotron emission to that of the total radiation ($(Q^-_{\rm syn} + Q^-_{\rm syn,C})/Q^-_{\rm rad}$) for both the two-phase accretion flow (right two panels; at $t = 1.8$–2.0) and the ADAF (right two panels; at $t = 7.8 - 8.0$). The first result we derive from this plot is that, the Comptonized synchrotron emission dominates for the regions within $40R_{\rm s}$, where most of the radiation comes from. This justifies our argument on the necessity of including synchrotron and the corresponding Comptonization processes. Besides, the radiation of hot accretion flow (both ADAF and the hot-phase medium of the two-phase accretion flow) is spatially extensive, covering a large volume. We note that, if the magnetic field is relatively stronger at high latitude regions where the β value is smaller compared to that of the mid-plane (e.g. in MHD simulations by Hawley & Krolik 2001; Hirose et al. 2009), then the spatial distribution of the radiation will be even more extensive and smooth. Additional emission from the cold clumps make the total emission of the two-phase accretion flow concentrates towards the equatorial plane.

We should point out that, the concentration of emission site of the two-phase accretion flow also depends on the wavebands observed. The hard X-ray emission should still be spatially extensive, as they are produced by the Compton scattering of the hot electrons. The soft X-ray and UV emission, on the other hand, will likely concentrates to the mid-plane, if the clumps are indeed most abundant there. Currently it remains unclear whether there will be more numerous smaller clumps formed, and whether these clumps can be supported to stay at higher altitude by the magnetic field. Further MHD simulations with higher spatial resolution will be required to clarify these questions.

3.3 Effects of plasma parameter β

In order to investigate the effect of magnetic field strength, we also run two additional models with $\beta = 100$ (**Run B**) and $\beta = 1$ (**Run B1**). The other model parameters are the same as those of the fiducial run. Fig. 9 shows the profiles of density, ion temperature and radial velocity at the mid-plane, before (averaged over the period $t = 1.3 - 1.4$; top panels) and after (averaged over the period $t = 1.8 - 2.0$; bottom panels) including the radiative cooling.

We first analyze the results without radiative cooling. If magnetic field is weak (**Run A** and **Run B**), the accretion flow will be gas pressure dominated. Consequently, there will be no significant differences between these simulations. The ion temperature of **Run B** is slightly higher, mainly because the gas pressure (roughly $\propto \rho T_{\rm i}$) increases as β increases, as the total pressure remains less affected. If magnetic field becomes strong enough, i.e. $\beta \sim 1$, its dynamical impact will be evident, even without considering the radiation processes. Indeed, When comparing **Run B1** with **Run A**, we find that the density becomes lower in low β case. This is because, we additionally put the magnetic pressure during the initial setup of the equilibrium (gravity against gas pressure gradient force) torus. Consequently, more fraction of the accreting material will be driven out as outflow due to the enhanced pressure gradient force at the early stage of evolution. The density will be lower and the accretion rate will be reduced. Besides, the ion temperature of **Run B1**, whose accretion rate is lower, is lower compared to that of **Run A**. This is because of weaker compression work ($p{\rm d}(1/\rho)$, which is proportional to density gradient; cf. the density profile in Fig. 9) done onto the gas in **Run B1**.

We then compare results with and without radiative cooling. The synchrotron emission, which provides the seed photons for the Compton scattering process, is more sensitive to the electron temperature than the magnetic field strength, i.e. we roughly have $Q_{\rm syn} \propto T_{\rm e}^7 B^3 \propto T_{\rm e}^7 P_{\rm mag}^{3/2}$ (This can be derived from Eq. 8, and note that ν_c is roughly proportional to $BT_{\rm e}^2$; NY95; See also Mehadevan 1997 for the dependence on $T_{\rm e}$). In this sense, The impact of including radiative cooling in **Run B**, whose electron temperature is the highest before considering radiative cooling (cf. top middle panels of Fig. 9), is significant, while the impact of including radiative cooling in **Run B1** is much weaker,

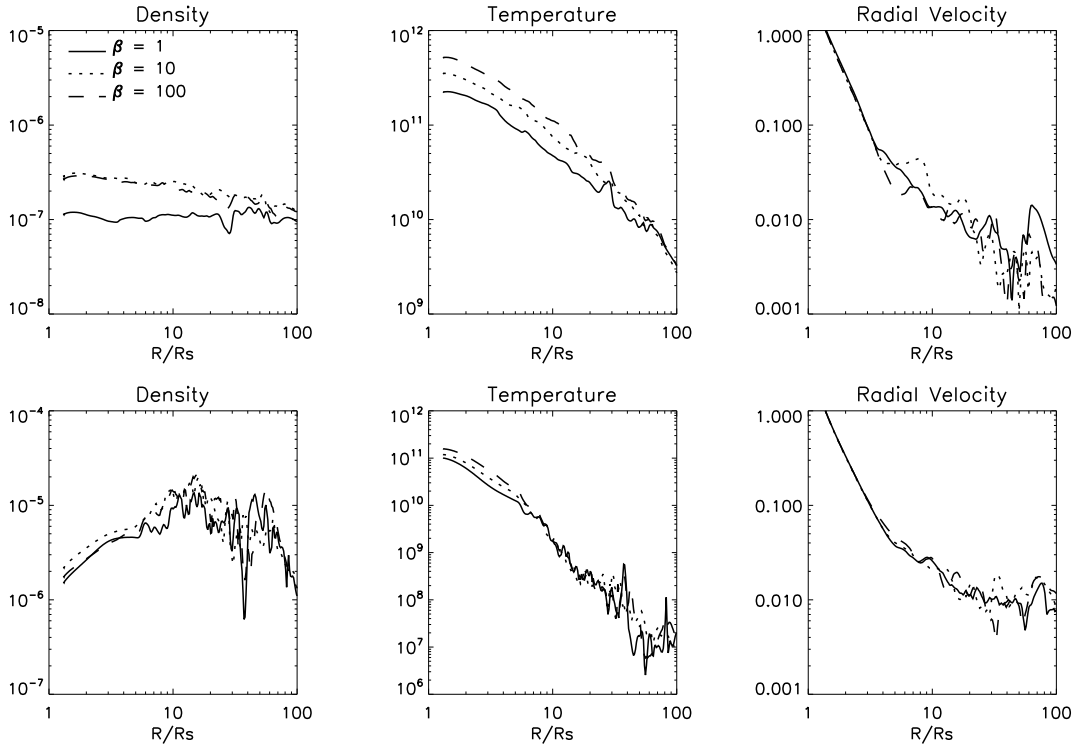

Figure 9. Comparison of the properties of simulations with different β values, i.e. the solid, dotted and dashed curves correspond to models with $\beta = 1, \beta = 10$ and $\beta = 100$, corresponding to **Run B1**, **Run A** and **Run B**, respectively. The upper panels show the averaged quantities (density, **temperature** and radial velocity) at the mid-plane over the period 1.3 – 1.4 (without radiative cooling), while bottom panels show averaged quantities over the period 1.8 – 2.0 (with radiative cooling).

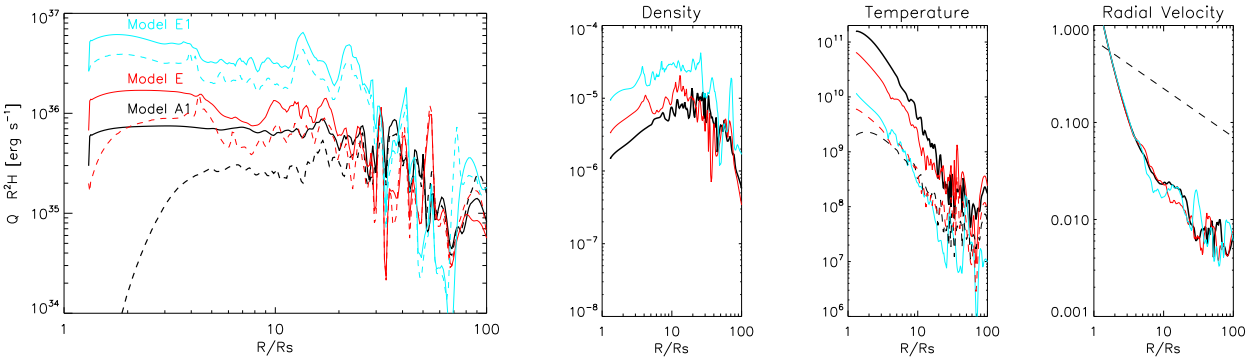

Figure 10. Comparison of simulations with different T_e/T_i values over period of t= 1.8 - 2.0 orbits. As labeled in the figure, **Run A1**, **Run E** and **Run E1** have $k = 1$, $k = 0.5$ and $T_e = T_i$ (sole temperature simulation), while they share the same other initial conditions. In the leftmost panel, the solid and dashed curves are the viscous heating rate and the total radiative cooling rate (both are multiplied by R^2 H). In the right three panels, show the density, temperature (solid line denotes the ions temperature, the dashed lines denotes the electrons temperature) and radial velocity in units of light speed (the dashed line denotes free fall speed.)

especially on the temperature of the gas. The difference of the total radiative cooling rates of the three runs are highly reduced, i.e. they differ by factors of $\lesssim 2$ for our chosen parameters. We note that the similarities of the three runs after including radiative cooling may be a coincidence, and should not be taken seriously. Radiative MHD simulations are required for a better understanding on the impacts of the magnetic fields, both dynamically (through magneto-rotational instability) and radiatively (through synchrotron emission).

Moreover, we also point out that our approach can only mimic the randomly-oriented turbulent magnetic fields, but not the global large scale one. The non-radiative simulations are different from those non-radiative MHD simulations, e.g. Stone & Pringle (2001). Their results show that the mass accretion rate depends on the initial magnetic field

strength, i.e. stronger magnetic field will lead to higher mass accretion rate. The reason is that, the Maxwell stress, which determines the capability of transporting angular momentum, will be stronger for cases with stronger vertical fields. In other words, stronger magnetic fields will generally have larger 'effective' α, while it is fixed to a constant in our HD simulations. Furthermore, in the MHD case, when radiative cooling becomes dominant, ADAF-like gaseous disk is shrieked in the vertical direction with frozen-in magnetic field, and magnetic pressure becomes relatively dominant in the cool disk. Hirose et al. (2009) showed that the plasma parameter β in coronal region became lower value than the disk region when radiative cooling becomes important. Therefore, the assumption of constant β will under-estimate synchrotron radiation.

3.4 The dependence on temperature ratio T_e/T_i

Obviously, only when radiative cooling becomes important in determining the dynamical structure of the accretion flow, the simulation results will be sensitive to the value of T_e/T_i (Mościbrodzka et al. 2009; Dibi et al. 2012).

From theoretical point of view, T_e/T_i depends mainly on two quantities. The first is the accretion rate. At sufficiently low accretion rate (e.g. the quiescent state and also the low luminosity hard state), the radiative cooling of electrons is insignificant, thus the T_e/T_i will be moderate (it depends on the energy deposition and also the adiabatic index differences between electrons and ions; cf. Yuan & Narayan 2014). As the accretion rate increases (i.e. normal hard state), the electrons will suffer additional radiative cooling and T_e will be reduced. T_i, on the other hand, remains nearly unaffected, mainly because the Couloumb collision is small compared to the viscous heating to ions at such moderate accretion rates. In other words, the value of T_e/T_i will become smaller in this regime. When the accretion rate is very high (e.g. the bright hard state and the intermediate state, i.e. the LHAF regime), the Couloumb coupling between electrons and ions, which scales as $\rho^2\ (T_i - T_e)$, is so strong that the temperature differences between electrons and ions are reduced, i.e. T_e/T_i will become moderately large again (see e.g. Yuan 2001; Xie et al. 2010). Note that for cases of SSD and possibly the cold clumps of the two-phase accretion flow, we will have $T_e = T_i$. Observationally we do observe an anti-correlation between electron temperature and the bolometric luminosity for the outburst of black hole X-ray binaries (e.g. Joinet et al. 2008; Miyakawa et al. 2008; Motta et al. 2009; Natalucci et al. 2014). The second quantity is the fraction of viscous heating that goes to electrons directly (see e.g. Xie & Yuan 2012 for a brief summary on constrains of this value). For given density and accretion rate, if more fraction of viscous heating goes to the electrons, obviously it will have a higher value of T_e/T_i, and the corresponding bolometric luminosity will also be enhanced.

We run two new simulations to investigate the impact of temperature ratio. With other parameters the same to those of **Run A1**, we set in **Run E** $k = 0.5$ and in **Run E1** $T_e = T_i$. The densities are high in these runs, and the radiative cooling is dynamically important, representing the bright hard (and also intermediate) state. As radiative cooling is triggered, differences are evident, as shown in Fig. 10 when a quasi-steady state is reached.

Reducing the differences between T_e and T_i (as in **Run E1** and **Run E**, compared to **Run A1**) is equivalent to enhance the coupling between electrons and ions. The T_e will then be increased, while the T_i will be reduced. The scale height of the hot accretion flow ($\propto (T_e + T_i)^{1/2}$) will also be reduced, which leads to an enhancement in gas density. The radiative cooling rate (synchrotron and its Comptonization, bremsstrahlung) will also be increased. All these results, as shown in Fig. 10, are easy to understand.

In the case of **Run E** series they start to form clumpy structures at lower accretion rate, i.e. they have more lower critical accretion rate of the purely hot accretion flow compared to those with $k = 1$ models. We also run some other simulations (not shown here) and the results confirm this point, such as the critical accretion rate is reduced to $\sim 0.006\ \dot{M}_{\rm Edd}$ in **Run E1**. The ratio between electron and ion temperature is the key point for the radiative cooling process, but it is very complex and depends on many factors and microphysical processes. Two-fluid (electrons and ions) radiative (MHD) simulations are needed to solve this problem. Only under this approach, we can investigate impact of the fraction of viscous heating to electrons, and come out a more reasonable T_e/T_i value (i.e. varies at different location and/or time).

4 SUMMARY AND DISCUSSIONS

In this paper, we present a number of two-dimensional hydrodynamical simulations of accretion flow on to a black hole, focusing on the impact of radiation cooling and state transitions. Compared to previous works (e.g. Das & Sharma 2013), our technical improvements includes: (1), the hot accretion flow in our simulations is two-temperature (NY95); (2), we follow the treatment of NY95 to consider the synchrotron emission and the corresponding Compton up-scattering process (see also Fragile & Meier 2009), which are crucial to generate the radiation observed in black hole X-ray binaries.

We summarize our major results as follows. Firstly, as the accretion rate increases, the truncated radius moves inward. This result is consistent with theoretical expectation (Esin et al. 1997) and the numerical simulations by Das & Sharma (2013). Secondly, when the accretion rate reaches the critical value $\dot{M} = 0.03\ \dot{M}_{\rm Edd} \approx 3\alpha\ \dot{M}_{\rm Edd}$ (Xie & Yuan 2012), we observe the formation of clumpy/filamentary structures within the hot medium, i.e. the whole accretion flow is likely to be in a two-phase accretion mode (see, e.g. Yuan 2003; Xie & Yuan 2012). As the accretion rate increases, these clumps grow and/or merge. Eventually the turbulent motions of the hot gas can not support them any longer, and they will settle down onto the mid-plane and form a thin disc. In other words, the clumpy accretion mode do exist before the eventually formation of the disc-corona configuration. It is speculated that this accretion mode may be responsible for the intermediate state of X-ray binaries (e.g. Yang et al. 2015).

We still lack direct evidences for the existence of cold clumps (or alternatively filaments, clouds), especially in BHBs. In AGNs, some clues can be derived from variability

studies. For example, in a broad absorption line (BAL; outflowing gas with velocity $\sim 0.1\ c$) quasar monitoring campaign, Capellupo et al. (2012) found that the variability favours the idea that those absorptions varies (on timescale of years) because of the movements of individual outflowing clouds (or at least substructures in the moving flow). Another example comes from NGC 5548 (Kaastra et al. 2014), where clumpy streams of ionized hot gas blocking the emission from the nucleus are observed.

Below we will highlight several notable shortages of our work, and discuss their consequences.

4.1 Oversimplification in the radiative cooling

In this work, we highly simplify the calculation of radiative cooling. The first is that, we use the critical frequency ν_c of the self-absorbed synchrotron emission to estimate the synchrotron cooling rate. Besides, we also use this frequency as the representative seed photon frequency for the Compton scattering process. Such approximation, which avoids any integration (in frequency ν), highly accelerates the computational speed. However, its accuracy is difficult to constrain.

More importantly, our Comptonization is based on the local Compton scattering approximation. In the optically thin medium as the case of hot accretion flow, seed photons can propagate a long distance from one location to another, and scatter with the hot electrons there. Such "global" Compton scattering process is not taken into account in our simulations. The global Comptonization process is recently examined in one-dimensional calculations, and it will make the electron temperature profile more flattened and the absolute $T_{\rm e}$ value reduced (by a factor of $\sim 1/3$. see e.g. Yuan , Xie & Ostriker 2009; Xie et al. 2010; Niedźwiecki et al. 2012). If we do not want to employ the computationally-expensive Monte Carlo technique, then one easy way to consider this effect is to create a correction factor profile from these numerical calculations and then apply it to the simulations here. However, such treatment is also very crude, and we omit it in this work.

4.2 Magnetic fields (large-scale ordered) in the hot accretion flow

In this work we used plasma β parameter to consider the effects of magnetic field (and correspondingly the synchrotron emission). Such approach has several limitations, which we will discuss below.

Firstly, this approach can not properly take into account the large-scale ordered magnetic fields. Plasma β can only provide a feasible and reasonable approximation for the consideration of the tangled, turbulent magnetic fields, but even in this case, it is not a constant within the accretion flow (Hawley & Krolik 2001). Besides, the dynamical structure of hot accretion flow will be highly revised if such large-scale magnetic field exist (Machida et al. 2006; Fragile & Meier 2009). The "effective" α will be highly enhanced if the accretion flow has large net magnetic flux (cf. Penna et al. 2013; Bai & Stone 2013). Besides, the large scale magnetic field may also be crucial for the formation and acceleration of the Poynting-dominated jet powered by the black hole spin (Blandford & Znajek 1977; Tchekhovskoy, Narayan & McKinney 2011), the disk-jet powered by the disk rotation (Yuan & Narayan 2014; Yuan et al. 2015), or jet powered by the radiation from supercritical accretion flow (Sadowski & Narayan 2015).

Secondly, one evolutionary stage of our simulations (e.g. in **Run A1**), before the eventual collapse into a cold thin disc, is the formation of the cold and dense clumpy/filamentary components. If these cold clumps are still coupled to the magnetic fields (valid likely only for small clumps), then the magnetic fields may service as natural barrier for the merger of those small clumps, i.e. the clumps will be confined by the large-scale magnetic fields. Besides, the large scale magnetic fields will provide additional vertical support for those cooling gas components, thus maintain them at higher altitude (Machida et al. 2006).

Finally, one interesting property related to the accumulation of the large scale global magnetic fields is that, they may help on the understanding of the the hysteretic cycle of black hole state transitions (Begelman & Armitage 2014 and references therein for alternative scenarios), i.e. the critical luminosity of the hard-to-soft transition is generally brighter than that of the soft-to-hard state. In the scenario proposed by Begelman & Armitage (2014), they expect that, during the hard state, vertical magnetic flux, which is generated near the truncated radius $R_{\rm tr}$, is advected inward and accumulates stochastically within the inner hot flow. Consequently the α will be large, leading to a higher critical luminosity for the hard-to-soft state transition (see also Yu et al. 2015 for the stability analysis of low-β hot accretion flows). On the other hand, the magnetic flux is gradually diffused out in the cold SSD during the soft state, thus the critical luminosity of the soft-to-hard state transition will be much lower. The numerical realization of this scenario is beyond the scope of current work.

4.3 Turbulent dissipation and corona heating

Another issue is related to the turbulent/viscous dissipation within the accretion flow. In this work (and also most of the hydrodynamical simulations of accretion flows), we adopt the α-viscosity prescription (Shakura & Sunyaev 1973), which assumes that the dissipation heating rate is proportional to the density of the gas. One consequence of this assumption is that, it assumes most of the "viscous" heating happens close to the mid-plane of the accretion flow.

Contradict to this assumption, recent MHD simulations, in which the magnetic reconnection is considered as the "physical" heating mechanism of the accretion disc, indicate that the vertical distribution of energy dissipation actually do not follow the density profile, but can extend to much higher height (e.g. Jiang, Stone & Davis 2014 and references therein). If this is indeed the case, then it will provide a natural heating mechanism for the corona in those disc-corona models (see e.g. Liu et al. 2002; Cao 2009), where they generally assume a significant fraction (of order $\sim 50\%$) of the "viscous" heating energy goes into the corona region. Besides, if such differences are taken into account, the mid-plane regions will be cooler, while the high altitude regions should be hotter.

5 ACKNOWLEDGMENTS

M.C.W. thanks Dr. De-Fu Bu, Dr. Zhen-Yi Cai and Prof. Feng Yuan for useful discussions. This work was supported in part by the Natural Science Foundation of China (grants U1231106, U1431228, 11133005, 11203057, 11233003, 11273042 and 11421303), the National Basic Research Program of China (2012CB821801), the Strategic Priority Research Program of the Chinese Academy of Sciences (XDB09000000), and the grant from 'the Fundamental Research Funds for the Central Universities'. This work made use of the High Performance Computing Resource in the Core Facility for Advanced Research Computing at Shanghai Astronomical Observatory. F.G.X. was also supported in part by the Youth Innovation Promotion Association of CAS (id. 2016243).

REFERENCES

Abramowicz M. A., Chen X., Kato S., Lasota J. P., Regev O., 1995, ApJ, 438, L37
Antonucci R., 2012, A&AT, 27, 557
Bai X. N., Stone J. M., 2013, ApJ, 767, 30
Balbus S. A., Hawley J. F., 1998, Rev. Mod. Phys., 70,1
Beckwith K., Hawley J. F., 2008, ApJ, 678, 1180
Begelman M. C., Armitage P. J., 2014, ApJ, 782, L18
Belloni T. M., 2010, in "The Jet Paradigm - From Microquasars to Quasars", ed. T. Belloni, Lecture Notes in Physics, Springer-Verlag, Berlin, 794, 53
Blandford R. D., Znajek R. L., 1977, MNRAS, 179, 433
Cao X., 2009, MNRAS, 394, 207
Capellupo D. M., Hamann F., Shields J. C., Rodriguez Hidalgo P., Barlow T. A., 2012, MNRAS, 422, 3249
Das U., Sharma P., 2013, MNRAS, 435, 2431
De Villiers J. P., Hawley J. F., Krolik J. H., 2003, ApJ, 599, 1238
Dermer C. D., Liang E. P., Canfield E., 1991, ApJ, 369, 410
Dibi S., Drappeau S., Fragile P. C., Markoff S., Dexter J., 2012, MNRAS, 426, 1928
Done C., 2014, in "Suzaku-MAXI 2014: Expanding the Frontiers of the X-ray Universe", proceedings of a conference held 19-22 February, 2014 at Ehime University, Japan. Eds. M. Ishida, R. Petre, and K. Mitsuda., p.300
Esin A. A., McClintock J. E., Narayan R., 1997, ApJ, 489, 865
Fender R. P., Belloni T. M., Gallo E., 2004, MNRAS, 355, 1105
Fragile P. C., Meier D. L., 2009, ApJ, 693, 771
Frank J., King A., Raine D., 2003, S&W, 42, 98
Hartnoll S. A., Blackman E. G., 2001, MNRAS, 324, 257
Hawley J. F., Balbus, S. A., Stone, J. M., 2001, ApJ, 554, L49
Hawley J. F., Krolik, J. H., 2001, ApJ, 548, 348
Hawley J. F., Guan X., Krolik J. H., 2011, ApJ, 738, 84
Hirose S., Krolik J. H., Blaes O., 2009, ApJ, 691,16
Ho L. C., 2008, ARA&A, 46, 475
Hubeny I., 1990, ApJ, 351, 632
Igumenshchev I. V., 2008, ApJ, 677, 317
Igumenshchev I. V., Abramowicz M. A., 1999, MNRAS, 303, 309
Igumenshchev I. V., Abramowicz M. A., 2000, ApJS, 130, 463
Igumenshchev I. V., Narayan R., Abramowicz M. A., 2003, ApJ, 592, 1042
Joinet A., Kalemci E., Senziani F., 2008, ApJ, 679, 655
Jiang Y. F., Stone J. M., Davis S. D., 2014, ApJ, 784,169
Kaastra, J. S. et al., 2014, Science, 345, 64
Li J., Ostriker J., Sunyaev R., 2013, ApJ, 767, 105
Liu B. F., Mineshige S., Shibata K., 2002, ApJ, 572, L173
Ma R. Y., 2012, MNRAS, 423L, 87
Mahadevan R., 1997, ApJ, 477, 585
Machida M., Nakamura K. E., Matsumoto R., 2004, PASJ, 56, 671
Machida M., Nakamura K. E., Matsumoto R., 2006, PASJ, 58, 193
McKinney J. C., 2006, MNRAS, 368, 1561
McKinney J. C., Tchekhovskoy A., Blandford R. D., 2012, MNRAS, 423, 3083
Miyakawa T., Yamaoka K., Homan J., Saito K., Dotani T., Yoshida A., Inoue H., 2008, PASJ, 60, 637
Mościbrodzka M., Gammie C. F., Dolence J. C, Shiokawa H., Leung P. K., 2009. ApJ, 706, 497
Motta S., Belloni T., Homan J., 2009, MNRAS, 400, 1603
Narayan R., 2005, Ap&SS, 300, 177
Narayan R., McClintock J. E., 2008, New Astron. Rev., 51, 733
Narayan R., Yi I., 1994, ApJ, 428, L13
Narayan R., Yi I., 1995, ApJ, 452, 710
Narayan R., Mahadevan R., Quataert E., 1998, in Abramowicz M. A., Bjornsson G., Pringle J. E., eds, Theory of Black Hole Accretion Discs. Cambridge Univ. Press, Cambridge, p. 148
Narayan R., Sadowski A., Penna R. F., Kulkarni A. K., 2012, MNRAS, 426, 3241
Natalucci L., Tomsick J. A., Bazzano A., 2014, ApJ, 780, 63
Niedźwiecki A., Xie F. G., Zdziarski A. A., 2012, MNRAS, 420, 1195
Ohsuga K., Mineshige S., 2011, ApJ, 736, 2
Ohsuga K., Mineshige S., Mori M., Kato Y., 2009, PASJ, 61, L7
Paczyński B., Wiita J., 1980, A&A, 88, 23
Papaloizou J. C. B., Pringle J. E., 1984, MNRAS, 208, 721
Penna R. F., Sadowski A., Kulkarni A. K., Narayan R., 2013, MNRAS, 428, 2255
Remillard R. A., McClintock J. E., 2006, ARA&A, 44, 49
Romanov, M. M., Ustyugova G. V., Koldoba A. V., Lovelace R. V. E., 2009, MNRAS, 399, 1802
Sądowski A., Narayan R., 2015, MNRAS, 454, 2372
Stone J. M., Norman M. L., 1992, ApJS, 80, 753
Stone J. M., Pringle J. E., Begelman M. C., 1999, MNRAS, 310, 1002
Stone J. M., Pringle J. E., 2001, MNRAS, 322, 461
Shakura N. I., Sunyaev R. A., 1973, A&A, 24, 337
Tchekhovskoy A., Narayan R., McKinney J. C., 2011, MNRAS, 418, L79
Wu Q. W., Cao X., Ho L. C., Wang D. X., 2013, ApJ, 700, 31
Xie F. G., Niedźwiecki A., Zdziarski A. A., Yuan F., 2010, MNRAS, 403, 170
Xie F. G., Yuan F., 2012, MNRAS, 427, 1580
Xie F. G., Yuan F., 2016, MNRAS, 456, 4377
Yang Q. X., Xie F. G., Yuan F., Zdziarski A. A., Gierlinski M., Ho L. C., Yu Z., 2015, MNRAS, 447, 1692
Yu X. F., Gu W. M., Liu T., Ma R. Y., Lu J. F., 2015, ApJ, 801, 47
Yuan F., 2001, MNRAS, 324, 119
Yuan F., 2003, ApJ, 594, L99
Yuan F., 2007, in L. C. Ho., J. M. Wang, eds., ASP conf. Ser., Vol. 373, The Central Engine of Active Galactic Nuclei. Astron. Soc. Pac., San Francisco, p.95
Yuan F., Bu D. F., 2010, MNRAS, 408, 1051
Yuan F., Bu D. F., Wu M. C., 2012, ApJ, 761, 130
Yuan F., Cui W., Narayan R., 2005, ApJ, 620, 905
Yuan F., Gan Z., Narayan R., Sadowski A., Bu D. F., Bai X. N., 2015, ApJ, 804, 101
Yuan F., Narayan R., 2014, ARA&A, 52, 529
Yuan F., Wu M. C., Bu D. F., 2012, ApJ, 761, 129
Yuan F., Xie F. G., Ostriker J. P., 2009, ApJ, 691, 98
Yuan F., Zdziarski A. A., 2004, MNRAS, 354, 953
Yuan F., Zdziarski A. A., Xue Y., Wu X. B., 2007, ApJ, 659, 541

Zdziarski A. A., Gierliński M., 2004, Progress Theor. Phys. Suppl., 155, 99